Matter and Radiation at Extremes | RESEARCH ARTICLE | scitation.org/journal/mre

Structural transitions of 4:1 methanol–ethanol mixture and silicone oil under high pressure

Cite as: Matter Radiat. Extremes 6, 038402 (2021); doi: 10.1063/5.0044893
Submitted: 20 January 2021 • Accepted: 24 March 2021 •
Published Online: 9 April 2021

Xiehang Chen,[1] Hongbo Lou,[1] Zhidan Zeng,[1] Benyuan Cheng,[1,2] Xin Zhang,[1] Ye Liu,[1] Dazhe Xu,[1] Ke Yang,[3] and Qiaoshi Zeng[1,4,a)]

AFFILIATIONS

[1]Center for High Pressure Science and Technology Advanced Research, Pudong, Shanghai 201203, People's Republic of China
[2]Shanghai Institute of Laser Plasma, Shanghai 201800, People's Republic of China
[3]Shanghai Synchrotron Radiation Facility, Shanghai 201800, People's Republic of China
[4]Jiangsu Key Laboratory of Advanced Metallic Materials, School of Materials Science and Engineering, Southeast University, Nanjing 211189, People's Republic of China

[a)]**Author to whom correspondence should be addressed:** zengqs@hpstar.ac.cn

ABSTRACT

A 4:1 (volume ratio) methanol–ethanol (ME) mixture and silicone oil are two of the most widely used liquid pressure-transmitting media (PTM) in high-pressure studies. Their hydrostatic limits have been extensively studied using various methods; however, the evolution of the atomic structures associated with their emerging nonhydrostaticity remains unclear. Here, we monitor their structures as functions of pressure up to ~30 GPa at room temperature using *in situ* high-pressure synchrotron x-ray diffraction (XRD), optical micro-Raman spectroscopy, and ruby fluorescence spectroscopy in a diamond anvil cell. No crystallization is observed for either PTM. The pressure dependence of the principal diffraction peak position and width indicates the existence of a glass transition in the 4:1 ME mixture at ~12 GPa and in the silicone oil at ~3 GPa, beyond which a pressure gradient emerges and grows quickly with pressure. There may be another liquid-to-liquid transition in the 4:1 ME mixture at ~5 GPa and two more glass-to-glass transitions in the silicone oil at ~10 GPa and ~16 GPa. By contrast, Raman signals only show peak weakening and broadening for typical structural disordering, and Raman spectroscopy seems to be less sensitive than XRD in catching these structural transitions related to hydrostaticity variations in both PTM. These results uncover rich pressure-induced transitions in the two PTM and clarify their effects on hydrostaticity with direct structural evidence. The high-pressure XRD and Raman data on the two PTM obtained in this work could also be helpful in distinguishing between signals from samples and those from PTM in future high-pressure experiments.

I. INTRODUCTION

Pressure is one of the most important fundamental thermodynamic parameters dictating the state of matter. Changes in the external pressure applied to a material will result in changes in interatomic spacing, and consequently electronic and atomic structures and various material properties can be significantly modified, sometimes in unexpected ways.[1,2] The static high pressures of up to hundreds of gigapascals obtainable with diamond anvil cells (DACs) open up a vast pressure dimension for exploration of new physics, chemistry, and materials science.[3,4] The degree of hydrostaticity of pressure not only has ramifications for the accurate determination of pressure but also has a strong effect on the deformation, stability, and phase transition paths of materials under compression and decompression.[5] Therefore, various pressure-transmitting media (PTM) have been employed to provide the different degrees of hydrostaticity required for materials studies and for synthesis in DACs. Gases and liquids do not support shear stress during a typical experimental time window (much longer than the shear stress relaxation time), and therefore they can maintain a pressure environment with identical stress from all directions, i.e., ideal hydrostaticity.[1] Unfortunately, all gases and liquids will inevitably solidify through phase transitions at critical high pressures, which causes degradation of hydrostaticity and the presence of differential stress components (pressure gradient) beyond so-called hydrostatic limit pressures.[6–8] Inert gases, such as He and Ne, are considered the best PTM owing to their stable chemical properties and low x-ray scattering background signals. However, they require specialized equipment for loading into DACs in the form of condensed liquids by compression and, in addition, He

and Ne will crystallize at 11.5 GPa[8] and 4.7 GPa[9] at room temperature, respectively. By contrast, liquid PTM are extensively used for DAC experiments owing to their ease of preparation and loading with comparable hydrostaticity at relatively low pressures.

The most commonly used liquid PTM are a 4:1 methanol–ethanol (ME) mixture and silicone oil (polydimethylsiloxane). Hydrostaticity of PTM is usually characterized by the pressure gradient within a sample chamber, which can be readily measured by the broadening of ruby fluorescence emission lines[7,10] or the pressure difference between ruby chips or balls at different locations inside the chamber.[11] The high-pressure hydrostaticity of the 4:1 ME mixture has been well studied, and has a reported hydrostatic limit of ~10.5 GPa during static compression.[11–15] However, some studies show a slight deviation from ideal hydrostaticity at ~5 GPa.[16] Silicone oil gives much more varied results for hydrostaticity. It has a higher viscosity (which facilitates sample loading) but similar hydrostaticity compared with the 4:1 ME mixture up to ~15 GPa.[17] Shen *et al.*[18] reported that silicone oil is superior to the 4:1 ME mixture even beyond 20 GPa. Hsieh[19] studied the thermal conductivities and elastic constants C_{11} of the 4:1 ME mixture and silicone oil under high pressure at room temperature, and the results suggested a fluid state of the silicone oil up to 23 GPa. By contrast, Angel *et al.*[15] examined the x-ray diffraction (XRD) peak width of quartz single crystals and observed the emergence of nonhydrostatic stress at ~9.8 GPa in the 4:1 ME mixture but at only ~0.9 GPa in silicone oil. Klotz *et al.*[11] measured the pressure difference between several ruby balls in silicone oil and observed the emergence of pressure gradient at ~3 GPa. Kirichenko *et al.*[20] estimated the solidification line of silicone oil to be 2–4 GPa at room temperature by measuring the resistance of an organic single crystal immersed in the oil. Murata *et al.*[21] experimentally determined the solidification pressure of silicone oil to be 3 GPa, using the standard deviation (σ vs pressure) of pressure in various locations inside the pressure cell. By measuring the specific heat capacity and thermal conductivity, Sandberg and Sundqvist[22,23] also claimed that silicone oil undergoes a glass transition at very low pressure of ~1 GPa. Tateiwa and Haga[24] used the ruby fluorescence emission line width under high pressure and low temperature and also demonstrated that hydrostaticity in silicone oil is worse than that in the 4:1 ME mixture at pressures above ~4 GPa.

The hydrostaticity limits in both liquid PTM are conjectured to be associated with solidification caused by pressure-induced glass transitions[7] or crystallization,[18,22] but this has yet to be confirmed by direct evidence.[17–19] In addition to ruby fluorescence spectroscopy, various other methods such as viscosity,[25] refractivity,[13] thermal properties,[19,22] elastic properties,[26] Raman spectroscopy,[14] and infrared spectroscopy[27] have been employed to study the 4:1 ME mixture and/or silicone oil. However, owing to the extremely low x-ray scattering ability of these two PTM, x-ray diffraction (XRD) signals from them are usually treated as weak background and ignored. Therefore, direct structural information from XRD associated with the development of hydrostaticity is still lacking, although this is critical for efforts to clarify the inconsistency of the hydrostaticity limits reported in the literature and to determine the underlying structural mechanism for the behavior under compression of these PTM.

In this work, we combine *in situ* high-pressure synchrotron XRD and micro-Raman spectroscopy to study the structural evolution of the 4:1 ME mixture and silicone oil under high pressure and room temperature through their hydrostaticity limits. The high-quality XRD patterns with careful background subtraction and Raman spectra of these two PTM reveal rich structural transitions, which are correlated well with the development of hydrostaticity.

II. EXPERIMENTAL

In situ high-pressure synchrotron XRD or Raman spectroscopy experiments at room temperature were performed on the 4:1 ME mixture and silicone oil using a symmetric DAC with a culet size of ~400 μm. T301 stainless steel was used for gaskets, which were pre-indented to ~20 GPa to form indents with a thickness of ~47 μm. The sample chamber was a ~150 μm diameter hole drilled in the center of a pre-indented indent in the gasket. The 4:1 ME mixture was prepared by mixing analytical reagent (AR) grade methanol (<0.1 vol. % water) with ethanol (<0.2 vol. % water). The silicone oil was a polydimethylsiloxane oil (Baysilone oil M1000) with a viscosity of 1000 mPa s at 25 °C (the viscosity depends on the mean molecular weight). Several tiny ruby balls[28] with similar sizes and almost identical initial fluorescence spectra were loaded along with the PTM samples. The R_1 line shift of ruby fluorescence was used for pressure calibration.[29] The pressure difference between ruby balls loaded at different locations inside the sample chamber of a DAC was used to estimate the pressure gradient, which is a sensitive and reliable indicator of the magnitude of a shear component (nonhydrostaticity).[11,16,30]

In situ high-pressure synchrotron XRD experiments were carried out on beamline 15U1 of the Shanghai Synchrotron Radiation Facility (SSRF) and on beamline 13-IDD of the Advanced Photon Source (APS) at Argonne National Laboratory (ANL). On beamline 15U1, the x-ray wavelength λ was 0.6199 Å and the beam size was ~4 × 10 μm^2, while on beamline 13-IDD, λ was 0.3220 Å and the beam size was ~2.5 × 3.5 μm^2. The data were collected by a MAR165 charge-coupled device (CCD) detector and a Pilatus1M CdTe detector on beamlines 15U1 and 13-IDD, respectively. Owing to the weak scattering ability of the 4:1 ME mixture and silicone oil, background signals from diamond anvils and air on the beam path are critical and were carefully collected before loading PTM samples into DACs, under identical experimental conditions to those used for the later measurements on the two PTM samples.

In situ high-pressure Raman spectroscopy experiments were performed using a micro-Raman spectroscopy system (inVia Reflex, Renishaw) with a 532 nm laser beam as the excitation source. The laser beam spot size was ~2 μm. The laser power was 83.3 mW, and the exposure time was 20 s and was accumulated twice for better signal. Testing with different laser powers did not show any obvious changes in the sample Raman signal.

It should be noted that all the XRD and Raman spectra data were collected consistently near the ruby ball at the sample chamber center to minimize signal fluctuations due to uncertainties in the sample position. The data were collected until the pressure was stabilized after a waiting time of ~15 min,[17] and this stabilization was also supported by the small pressure difference from the same ruby ball measured before and after XRD or Raman data collection.

III. RESULTS AND DISCUSSION

A. 4:1 methanol–ethanol mixture

The hydrostaticity of the 4:1 ME mixture with increasing pressure was characterized by the pressure differences between three

ruby balls at different locations inside the sample chamber (shown as the inset in Fig. 1): two balls were near the center, and the other was close to the edge of the chamber. The three balls show almost identical pressures below ~12 GPa, and then nonhydrostaticity sets in and quickly develops with increasing pressure above ~12 GPa, which is manifested by the diverging pressures of the individual ruby balls and the increased standard deviation σ among them, as shown in Fig. 1. The most significant pressure difference between ruby 1 and ruby 3 reaches ~2.3 GPa at 22.2 GPa. The positions of the ruby balls remain the same over the entire experiment, and the results are quite reproducible in several repeated experiments. The abrupt change in σ suggests a transition from hydrostatic to nonhydrostatic conditions at ~12 GPa, which typically characterizes a liquid-to-glass transition.

Figure 2(a) shows the XRD patterns of the 4:1 ME sample after subtraction of background signals during compression up to 22.2 GPa. The starting pressure was set at ~0.8 GPa to securely seal the 4:1 ME mixture in the DAC. At 0.8 GPa, the XRD pattern of the 4:1 ME mixture displays only one pronounced but broad diffuse peak located at ~1.83 Å^{-1}. With increasing pressure, this principal peak shifts to a higher diffraction vector q and becomes obviously broader above ~11.3 GPa. Meanwhile, a second weak peak emerges at ~4.6 Å^{-1} and grows with pressure. Nevertheless, at the highest pressure of ~22.2 GPa in this work, the second peak is still much weaker than the principal peak. Besides, the intensity between 2.5 and 4.0 Å^{-1} also increases slightly above 4.6 GPa, which indicates another transition with subtle structural changes taking place above 4.6 GPa and is consistent with the previously reported slight deviation from ideal hydrostaticity above 5 GPa in the 4:1 ME mixture.[16] There is no sharp Bragg diffraction peak up to 22.2 GPa, which rules out the pressure-induced crystallization reported in inert gasses[8,9] and most pure liquids.[31] When the pressure is released to ~0.8 GPa during decompression, the diffraction pattern of the 4:1 ME mixture shows peak position and shape almost identical to those of the initial state at ~0.8 GPa during compression, which means that the phase transitions are reversible, as expected for typical glass or liquid-to-liquid transitions. For quantitative analysis, we focus only on the relatively intense principal peak. A Voigt line profile was used to fit the principal diffraction peak position q_1 and peak width [full width at half maximum (FWHM)] after subtracting a linear baseline. Figure 2(b) shows q_1 as a function of pressure, and it can be seen that it initially increases rapidly with pressure, with a slight change in slope at around 4.6 GPa, and then the rate of increase slows down above ~11.3 GPa. The peak width (FWHM), as shown in Fig. 2(c), first decreases gently below 4.6 GPa, and then turns to increase slightly. Above ~11.3 GPa, the FWHM increases steeply with pressure. This result also suggests that there may be a weak transition at ~4.6 GPa and a sharp transition at ~11.3 GPa. According to the empirical cubic power-law scaling of the diffraction peak and sample volume for liquids,[32,33] the sample volume can be estimated from the diffraction peak position, $V \propto (1/q)^3$, as shown in Fig. 2(d). The third-order Birch–Murnaghan equation of state (BM-EOS)[34] cannot describe the compression behavior over the entire pressure range, and therefore the low-pressure (<11.3 GPa) and high-pressure (>1.3 GPa) regions are fitted separately by the third-order BM-EOS with a transition point at ~11.3 GPa, The EOS fitting yields an isothermal bulk modulus $B_0 = 2.5 \pm 0.1$ GPa and pressure derivative $B_0' = 4.6 \pm 0.1$ GPa below 11.3 GPa and $B_0 = 16.3 \pm 1.5$ GPa, $B_0' = 7.2 \pm 0.8$ GPa above 11.3 GPa. The volume in the low-pressure region estimated by the cubic power law coincides well with previous data obtained by an optical imaging technique.[35] Considering the lack of any sharp diffraction Bragg diffraction peaks, the transition suggested by the kinks at ~11 GPa in peak shifting and broadening with different bulk moduli is quite consistent with the reported glass transition pressure at ~10.5 GPa obtained by other methods.[11,15]

To derive more structural information about the glass transition of the 4:1 ME mixture, an *in situ* high-pressure Raman spectroscopy experiment was performed up to ~32 GPa. The high-pressure Raman spectra of the 4:1 ME mixture are shown in Fig. 3. All the Raman modes of the 4:1 ME can be assigned to either pure methanol or pure ethanol.[14,36] All the Raman peaks show gradual broadening and blueshifting under compression, following an almost linear relationship with pressure, even crossing the glass transition, as reported previously.[14] The reversible peak profile and position during decompression suggest that the structural changes are reversible, as also suggested by the XRD results. Since the Raman spectra of the 4:1 ME mixture have been extensively reported and analyzed before (<20 GPa),[14,36–39] no detailed analysis is repeated in this work. However, it should be noted that in contrast to the new features (enhanced broad peaks) observed in the XRD results, no new Raman peak emerges during compression or decompression. The apparent relative intensity change between the peaks at ~2800 and ~2900 cm^{-1} (originating from CH stretching modes and Fermi coupling[14,36]) occurs continuously from the very beginning of compression (when the mixture is still in the liquid state); however, it could not be directly associated with the hydrostaticity to nonhydrostaticity transition at ~11.3 GPa. These results indicate that the Raman spectrum may not be as sensitive as XRD in catching structural changes such as a glass transition of the 4:1 ME mixture under high pressure.[14]

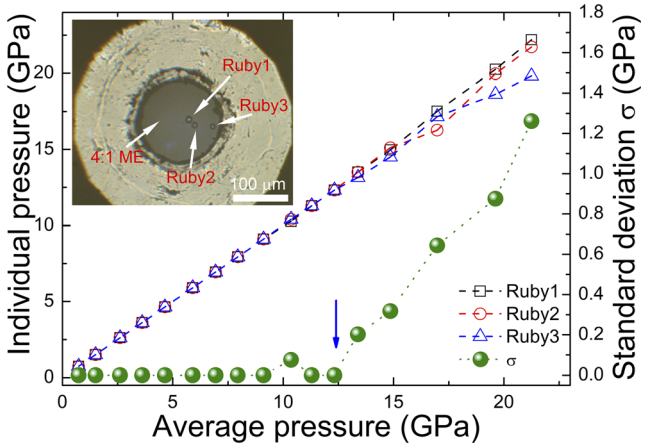

FIG. 1. Pressure dependence of hydrostaticity inside the sample chamber of a DAC with a 4:1 ME mixture as the PTM. The hydrostaticity was characterized by the different pressures (open symbols, left vertical axis) obtained from three ruby balls at different locations inside the sample chamber and their standard deviation (solid symbols, right vertical axis). The arrow marks the onset pressure of nonhydrostaticity. The inset shows an image of the 4:1 ME mixture at ~9 GPa along with the three ruby balls inside the DAC.

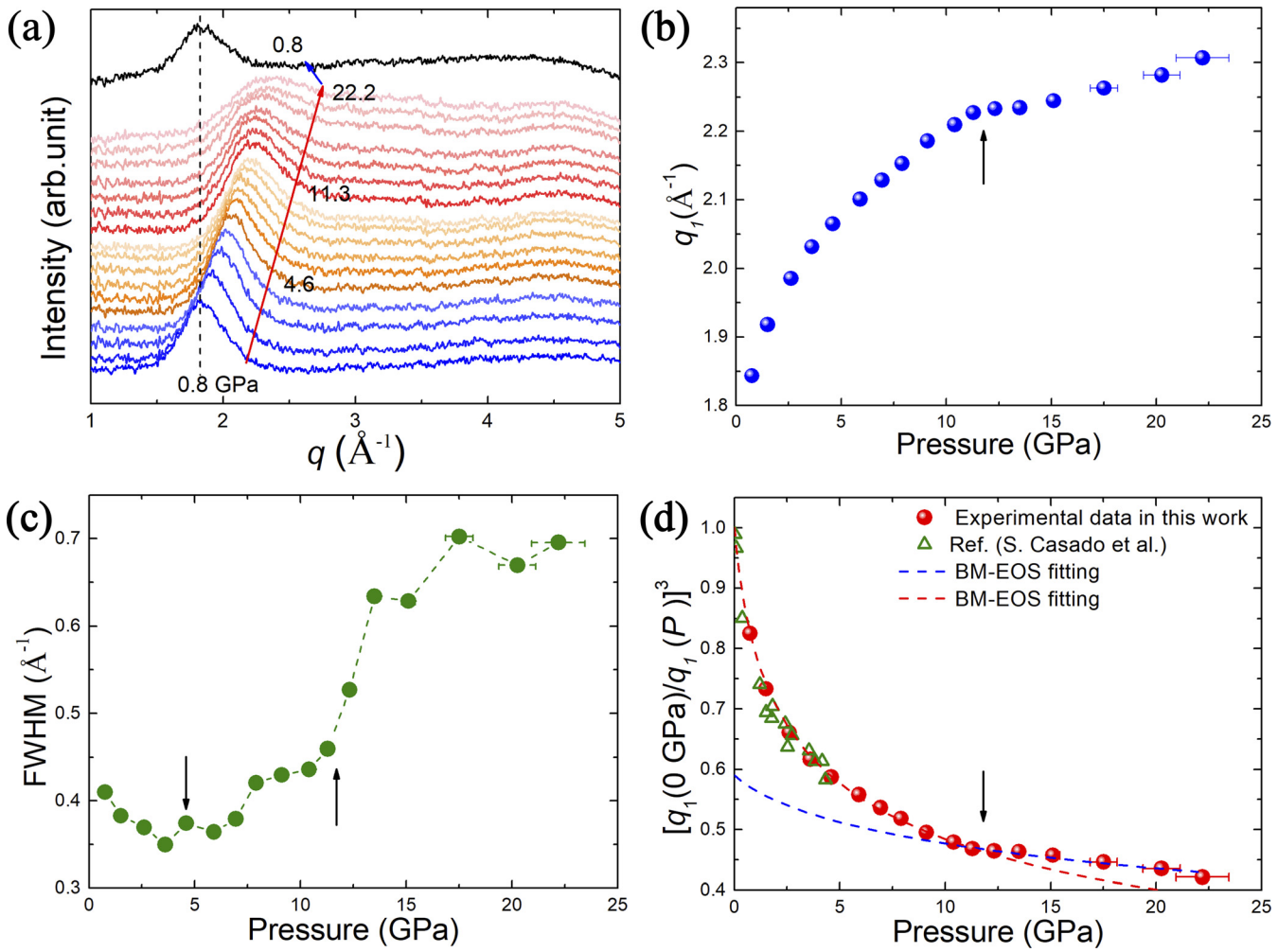

FIG. 2. *In situ* high-pressure XRD of the 4:1 ME mixture. (a) XRD patterns of the 4:1 ME mixture from 0.8 GPa to 22.2 GPa during compression and decompression. The numbers on the patterns denote their pressures, and the red and blue solid lines indicate the compression and decompression directions, respectively. (b) and (c) Pressure dependences of the principal diffraction peak position and peak width. (d) Pressure dependence of the sample volume estimated by the cubic power law and compared with volume data from the literature.[35] The dashed lines are the third-order BM-EOS fittings of the volume data obtained in this work below 12 GPa (red dashed line) and above 12 GPa (blue dashed line). The arrows in (b)–(d) mark the critical pressures for possible transitions. The horizontal error bars represent pressure uncertainty due to nonhydrostaticity. The fitting errors of the peaks are smaller than the symbol size.

B. Silicone oil

The behavior of the hydrostaticity of the silicone oil with increasing pressure was characterized by the pressure differences between two ruby balls located at the center and the edge of the sample chamber, respectively (shown as the inset in Fig. 4). Below 3 GPa, the two ruby balls show identical pressures. A pressure difference emerges above 3 GPa and quickly reaches a flat region, after which it remains almost constant at ~0.3 GPa from ~4 to ~8 GPa. This observation suggests a liquid-to-solid transition (most likely a glass transition) at ~3 GPa, in line with some previous reports.[22–24] Above ~10 GPa, the pressure difference turns to increase sharply with further compression; for example, the standard deviation of the pressure, σ, reaches ~2.4 GPa at ~20 GPa and ~4 GPa at ~29 GPa, which is quite consistent with previous results.[11] Although the gasket hole gradually expanded above 23 GPa, the ruby balls did not move obviously and kept an almost constant distance between each other. Repeated experiments also show consistent results, suggesting σ to be a reliable indicator for hydrostaticity and pressure gradient. Compared with the 4:1 ME mixture, it is clear that nonhydrostaticity emerges in the silicone oil at a much lower pressure (~3 GPa) and reaches slightly higher values of the pressure gradient above 10 GPa (an approximately linear gradient of ~0.036 GPa/μm in the 4:1 ME mixture vs ~0.046 GPa/μm in the silicone oil at an average chamber pressure of ~20 GPa). These results demonstrate that the silicone oil has worse hydrostaticity than the 4:1 ME mixture below 20 GPa. It is most likely that silicone oil

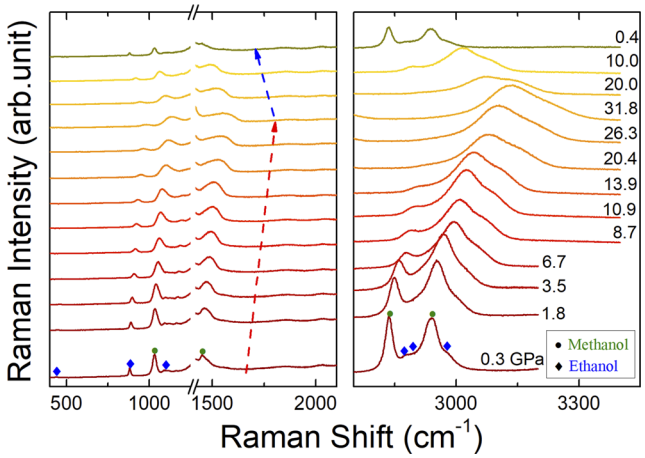

FIG. 3. *In situ* high-pressure Raman spectra of the 4:1 ME mixture during compression and decompression. The spectra are collected in two separate regions owing to the limited coverage of the Raman spectrometer. The scale break on the horizontal axis omits the spectrum near the strong diamond Raman peak at ~1332 cm^{-1}. The red and blue dashed lines indicate the compression and decompression processes, respectively. The solid circles mark the peaks from methanol, while the solid diamond symbols mark the peaks from ethanol.

undergoes a glass transition at ~3 GPa and complicated stress relaxation or hardening behavior caused by several glass-to-glass transitions above ~3 GPa.

Figure 5(a) shows the *in situ* high-pressure XRD patterns of the silicone oil up to 30 GPa. These patterns show more features than those of the 4:1 ME mixture. The XRD pattern at low pressures displays three visible broad diffuse peaks located at q_1 = ~0.9 Å^{-1}, q_2 = ~1.5 Å^{-1}, and q_3 = ~3.7 Å^{-1}, respectively. However, the three

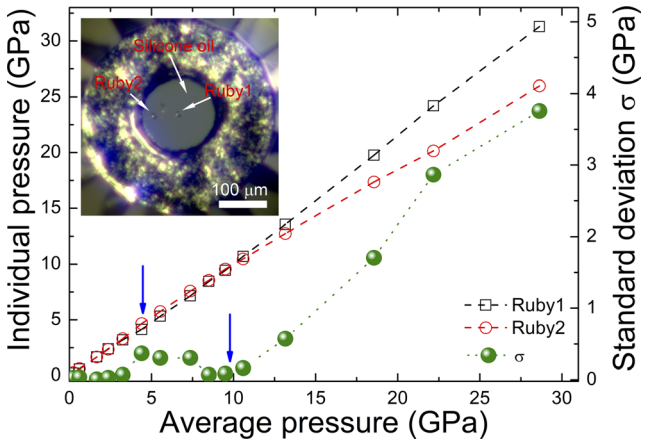

FIG. 4. Pressure dependence of hydrostaticity inside the sample chamber of a DAC with silicone oil as the PTM. The hydrostaticity was characterized by the different pressures (open symbols, left vertical axis) obtained from two ruby balls near the center and edge of the sample chamber and their standard deviation (solid symbols, right vertical axis). The arrows mark the pressures at dramatic changes in hydrostaticity. The inset shows an image of the silicone oil at ~1 GPa along with the two ruby balls inside the DAC.

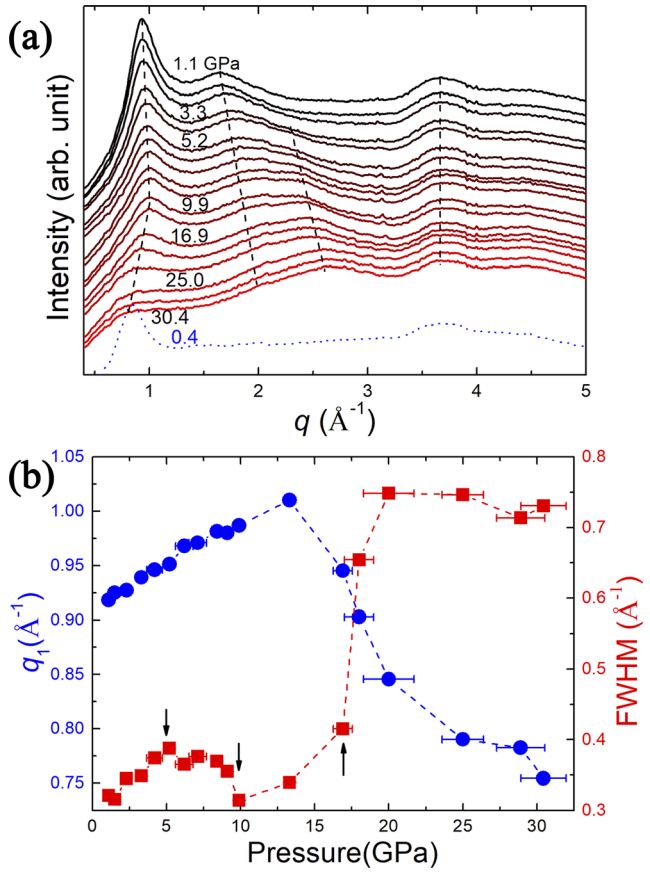

FIG. 5. *In situ* high-pressure XRD of silicone oil. (a) XRD patterns of silicone oil from 1.1 GPa to 30.4 GPa during compression and decompression to ~0.4 GPa. The black dashed lines are guides to the eye to show the trend in the shift of peak position with increasing pressure. The numbers on the patterns denote their pressures. The blue dotted pattern is at ~0.4 GPa during decompression. (b) Pressure dependence of the principal diffraction peak position (solid blue circles, left vertical axis) and peak width (solid red squares, right vertical axis) as obtained by fitting the principal XRD peaks using a Voigt line profile. The arrows mark the critical pressures for possible transitions. The horizontal error bars represent pressure uncertainty due to non-hydrostaticity. The fitting errors of the peaks are smaller than the symbol size.

peaks evolve quite differently from each other with increasing pressure. The first peak (the principal peak) first moves to higher q values below ~13 GPa, then turns backward in the direction of lower q with further compression, which is quite unusual for compression of most liquids or glasses and could only be caused by a transition between distinct structures rather than a glass-transition-induced solidification. The intensity weakens and the width broadens significantly during the entire compression process up to 30.4 GPa for the principal peak. The second peak shifts normally in the direction of higher q and becomes weaker as the highest pressure is approached, without apparent kinks. The third peak surprisingly remains almost intact during compression in terms of its shape and position, which could be attributed to some rigid intramolecular structures. Another new peak (or shoulder) at ~2.5 Å^{-1} emerges between 3 and 5 GPa and then remains broad and weak up to 30 GPa. Splitting of the second diffraction peak is usually a feature of a liquid-to-glass transition with

enhanced medium-range order.[40] These changes in XRD patterns suggest rich structural phase transitions in the silicone oil, which is much more complicated behavior than that of a single glass transition or crystallization as suggested previously.[7,18,22] After release of pressure to ~0.4 GPa, the XRD pattern recovers, but with weaker signals, especially for the second peak, which suggests a possible structural hysteresis. Given its high intensity and rich variation, quantitative analysis with peak fitting using a Voigt line profile was conducted only on the principal peak, as shown in Fig. 5(b). The peak position q_1 shows slight changes in slope with pressure below ~13 GPa; however, these are too weak to reflect the overall change in XRD patterns, as shown in Fig. 5(a). The most remarkable change in q_1 vs pressure is the sharp kink at ~13 GPa. This is close to, but not coincident with, the sharp increase in nonhydrostaticity (~10 GPa) observed from the ruby pressure gradient shown in Fig. 4. This inconsistency suggests that the behavior of the principal peak may involve complicated changes rather than simply reflecting a glass transition. By contrast, the width of the principal peak seems to be more sensitive to structural changes, with an almost one-to-one correspondence to the changes in XRD pattern features. Since the XRD patterns show anomalous changes rather than a simple densification effect during compression, the sample volume changes cannot be reliably estimated using the cubic power law.[41]

By contrast, *in situ* high-pressure micro-Raman spectra of the silicone oil only exhibit continuous peak weakening and broadening from the beginning of compression, without any new peaks emerging during compression (Fig. 6). The recoverable peak profile after full pressure release to ~0.2 GPa indicates that the structural changes in the silicone oil during compression are likely reversible. Similar to the case of the 4:1 ME mixture, two intense Raman peaks between 2800 and 3000 cm^{-1} continuously change their relative intensity during compression; however, they also seem not to be directly associated with the structural transitions in the silicone oil.

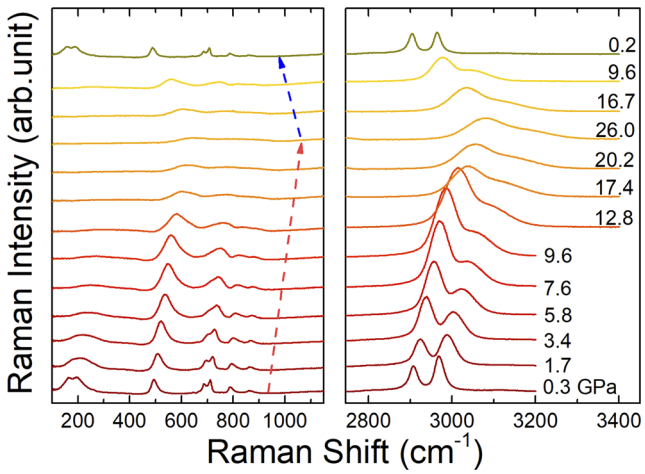

FIG. 6. *In situ* high-pressure Raman spectra of silicone oil during compression and decompression. The spectra are collected in two separate regions owing to the limited coverage of the Raman spectrometer. The red and blue dashed lines indicate the compression and decompression processes, respectively.

IV. CONCLUSION

From a comprehensive study combining ruby fluorescence spectroscopy, *in situ* high-pressure synchrotron XRD, and optical micro-Raman spectroscopy in DACs, atomic structural information associated with the development of hydrostaticity has been obtained for the two most commonly used liquid PTM for high-pressure experiments, namely, a 4:1 ME mixture and silicone oil. It has been shown that although the pressure gradients in the two PTM are comparable, the 4:1 ME mixture is a better hydrostatic PTM than the silicone oil below 20 GPa. The continuous peak broadening and absence of new sharp peaks in both XRD and Raman spectra rule out the possibility of pressure-induced crystallization in both PTM. A pressure-induced glass transition, which accounts for the emergence of nonhydrostaticity, occurs at ~11 to 12 GPa in the 4:1 ME mixture and ~3 GPa in the silicone oil, and below these pressures both PTM can be considered to be ideally hydrostatic. Besides glass transitions, a possible liquid-to-liquid transition is suggested at ~5 GPa in the 4:1 ME mixture, according to the kink in the principal diffraction peak width as a function of pressure. For the silicone oil, there are another two possible structural transitions at ~10 and ~16 GPa, associated with the anomalous change of pressure gradient and the pressure dependence of the principal diffraction peak position and width. By contrast, Raman signals seem to be not as sensitive as XRD in catching the structural transitions related to hydrostaticity variations in both PTM. These results provide direct evidence for the rich pressure-induced structural transitions in the two PTM, which helps clarify the inconsistency in previous studies regarding the underlying mechanism for the development of a pressure gradient. Moreover, the *in situ* high-pressure XRD patterns and Raman spectra collected up to 20–30 GPa also provide important reference data for future high-pressure studies to distinguish signals from samples and those from PTM and to estimate the influence of the latter on sample signals, especially when the samples have weak XRD or Raman signals owing to their low scattering cross-sections or disordered structures.

ACKNOWLEDGMENTS

This work was supported by the National Natural Science Foundation of China (Grant Nos. 51871054 and U1930401). The XRD experiments were performed on beamline 15U1 of the Shanghai Synchrotron Radiation Facility (SSRF) and on beamline 13 ID-D of GSECARS at the Advanced Photon Source (APS), Argonne National Laboratory (ANL), USA. The use of beamline 13-ID-D at the APS was supported by the National Science Foundation (NSF)–Earth Sciences (Grant No. EAR-1634415) and the Department of Energy (DOE)–GeoSciences (Grant No. DEFG02-94ER14466). The APS was supported by the DOE Office of Science (Grant No. DE-AC02-06CH11357).

DATA AVAILABILITY

The data that support the findings of this study are available from the corresponding author upon reasonable request.

REFERENCES

[1]H.-K. Mao, X.-J. Chen, Y. Ding, B. Li, and L. Wang, "Solids, liquids, and gases under high pressure," Rev. Mod. Phys. **90**, 015007 (2018).

[2]L. Zhang, Y. Wang, J. Lv, and Y. Ma, "Materials discovery at high pressures," Nat. Rev. Mater. **2**, 17005 (2017).
[3]H.-K. Mao, B. Chen, J. Chen, K. Li, J.-F. Lin, W. Yang, and H. Zheng, "Recent advances in high-pressure science and technology," Matter Radiat. Extremes **1**, 59 (2016).
[4]B. Li, C. Ji, W. Yang, J. Wang, K. Yang, R. Xu, W. Liu, Z. Cai, J. Chen, and H.-k. Mao, "Diamond anvil cell behavior up to 4 Mbar," Proc. Natl. Acad. Sci. U. S. A. **115**, 1713 (2018).
[5]V. I. Levitas, "High pressure phase transformations revisited," J. Phys.: Condens. Matter **30**, 163001 (2018).
[6]P. W. Bridgman and E. A. Mason, "Collected experimental papers of P. W. Bridgman," Am. J. Phys. **33**, 516 (1965).
[7]G. J. Piermarini, S. Block, and J. D. Barnett, "Hydrostatic limits in liquids and solids to 100 kbar," J. Appl. Phys. **44**, 5377 (1973).
[8]J. M. Besson and J. P. Pinceaux, "Melting of helium at room temperature and high pressure," Science **206**, 1073 (1979).
[9]L. W. Finger, R. M. Hazen, G. Zou, H. K. Mao, and P. M. Bell, "Structure and compression of crystalline argon and neon at high pressure and room temperature," Appl. Phys. Lett. **39**, 892 (1981).
[10]R. A. Forman, G. J. Piermarini, J. D. Barnett, and S. Block, "Pressure measurement made by the utilization of ruby sharp-line luminescence," Science **176**, 284 (1972).
[11]S. Klotz, J.-C. Chervin, P. Munsch, and G. Le Marchand, "Hydrostatic limits of 11 pressure transmitting media," J. Phys. D: Appl. Phys. **42**, 075413 (2009).
[12]P. W. Bridgman, "Further rough compressions to 40,000 Kg/Cm: Especially certain liquids," Am. Acad. Arts Sci. **77**, 129 (1949).
[13]J. H. Eggert, L. w. Xu, R. z. Che, L. c. Chen, and J. f. Wang, "High pressure refractive index measurements of 4:1 methanol:ethanol," J. Appl. Phys. **72**, 2453 (1992).
[14]X. B. Wang, Z. X. Shen, S. H. Tang, and M. H. Kuok, "Near infrared excited micro-Raman spectra of 4:1 methanol–ethanol mixture and ruby fluorescence at high pressure," J. Appl. Phys. **85**, 8011 (1999).
[15]R. J. Angel, M. Bujak, J. Zhao, G. D. Gatta, and S. D. Jacobsen, "Effective hydrostatic limits of pressure media for high-pressure crystallographic studies," J. Appl. Crystallogr. **40**, 26 (2007).
[16]D. M. Adams, R. Appleby, and S. K. Sharma, "Spectroscopy at very high pressures. X. Use of ruby R-lines in the estimation of pressure at ambient and at low temperatures," J. Phys. E: Sci. Instrum. **9**, 1140 (1976).
[17]D. D. Ragan, D. R. Clarke, and D. Schiferl, "Silicone fluid as a high-pressure medium in diamond anvil cells," Rev. Sci. Instrum. **67**, 494 (1996).
[18]Y. Shen, R. S. Kumar, M. Pravica, and M. F. Nicol, "Characteristics of silicone fluid as a pressure transmitting medium in diamond anvil cells," Rev. Sci. Instrum. **75**, 4450 (2004).
[19]W.-P. Hsieh, "Thermal conductivity of methanol-ethanol mixture and silicone oil at high pressures," J. Appl. Phys. **117**, 235901 (2015).
[20]A. S. Kirichenko, A. V. Kornilov, and V. M. Pudalov, "Properties of polyethylsiloxane as a pressure-transmitting medium," Instrum. Exp. Tech. **48**, 813 (2005).
[21]K. Murata, K. Yokogawa, H. Yoshino, S. Klotz, P. Munsch, A. Irizawa, M. Nishiyama, K. Iizuka, T. Nanba, T. Okada, Y. Shiraga, and S. Aoyama, "Pressure transmitting medium Daphne 7474 solidifying at 3.7 GPa at room temperature," Rev. Sci. Instrum. **79**, 085101 (2008).
[22]O. Sandberg and B. Sundqvist, "Thermal properties of two low viscosity silicon oils as functions of temperature and pressure," J. Appl. Phys. **53**, 8751 (1982).
[23]B. Sundqvist, "Comment on "Characteristics of silicone fluid as a pressure transmitting medium in diamond anvil cells" [Rev. Sci. Instrum. **75**, 4450 (2004)]," Rev. Sci. Instrum. **76**, 057101 (2005).
[24]N. Tateiwa and Y. Haga, "Evaluations of pressure-transmitting media for cryogenic experiments with diamond anvil cell," Rev. Sci. Instrum. **80**, 123901 (2009).
[25]B. Grocholski and R. Jeanloz, "High-pressure and -temperature viscosity measurements of methanol and 4:1 methanol:ethanol solution," J. Chem. Phys. **123**, 204503 (2005).
[26]X. Wang, C. Chen, X. Huang, J. Wang, M. Yao, K. Wang, F. Huang, B. Han, Q. Zhou, and F. Li, "Acoustic and elastic properties of silicone oil under high pressure," RSC Adv. **5**, 38056 (2015).
[27]J. C. Chervin, B. Canny, J. M. Besson, and P. Pruzan, "A diamond anvil cell for IR microspectroscopy," Rev. Sci. Instrum. **66**, 2595 (1995).
[28]J. C. Chervin, B. Canny, and M. Mancinelli, "Ruby-spheres as pressure gauge for optically transparent high pressure cells," High Pressure Res. **21**, 305 (2001).
[29]H. K. Mao, J. Xu, and P. M. Bell, "Calibration of the ruby pressure gauge to 800 kbar under quasi-hydrostatic conditions," J. Geophys. Res. **91**, 4673, https://doi.org/10.1029/jb091ib05p04673 (1986).
[30]D. Staško, J. Prchal, M. Klicpera, S. Aoki, and K. Murata, "Pressure media for high pressure experiments, Daphne oil 7000 series," High Pressure Res. **40**, 525 (2020).
[31]L. E. Reeves, G. J. Scott, and S. E. Babb, Jr., "Melting curves of pressure-transmitting fluids," J. Chem. Phys. **40**, 3662 (1964).
[32]O. F. Yagafarov, Y. Katayama, V. V. Brazhkin, A. G. Lyapin, and H. Saitoh, "Energy dispersive x-ray diffraction and reverse Monte Carlo structural study of liquid gallium under pressure," Phys. Rev. B **86**, 174103 (2012).
[33]P. Chirawatkul, A. Zeidler, P. S. Salmon, S. i. Takeda, Y. Kawakita, T. Usuki, and H. E. Fischer, "Structure of eutectic liquids in the Au–Si, Au–Ge, and Ag–Ge binary systems by neutron diffraction," Phys. Rev. B **83**, 014203 (2011).
[34]F. Birch, "Elasticity and constitution of the earth interior," J. Geophys. Res. **57**, 227, https://doi.org/10.1029/jz057i002p00227 (1952).
[35]S. Casado, H. E. Lorenzana, M. Cáceres, M. Taravillo, and V. G. Baonza, "Direct measurement of the liquid 4:1 methanol–ethanol equation of state up to 5 GPa," High Pressure Res. **28**, 637 (2008).
[36]V. Lemos and F. Camargo, "Effects of pressure on the Raman spectra of a 4:1 methanol–ethanol mixture," J. Raman Spectrosc. **21**, 123 (1990).
[37]A. Serrallach, R. Meyer, and H. H. Günthard, "Methanol and deuterated species: Infrared data, valence force field, rotamers, and conformation," J. Mol. Spectrosc. **52**, 94 (1974).
[38]Y. Mikawa, J. W. Brasch, and R. J. Jakobsen, "Polarized infrared spectra of single crystals of ethyl alcohol," Spectrochim. Acta, Part A **27**, 529 (1971).
[39]I. Artaki, M. Bradley, T. W. Zerda, and J. Jonas, "NMR and Raman study of the hydrolysis reaction in sol-gel processes," J. Phys. Chem. **89**, 4399 (1985).
[40]B. W. van de Waal, "On the origin of second-peak splitting in the static structure factor of metallic glasses," J. Non-Cryst. Solids **189**, 118 (1995).
[41]Q. S. Zeng, Y. Kono, Y. Lin, Z. D. Zeng, J. Y. Wang, S. V. Sinogeikin, C. Park, Y. Meng, W. G. Yang, H. K. Mao, and W. L. Mao, "Universal fractional noncubic power law for density of metallic glasses," Phys. Rev. Lett. **112**, 185502 (2014).